Violation of classical inequalities by photon frequency filtering

C. Sánchez Muñoz,* E. del Valle, C. Tejedor, and F. P. Laussy†
Departamento de Física Teórica de la Materia Condensada and Condensed Matter Physics Center (IFIMAC), Universidad Autónoma de Madrid, E-28049 Madrid, Spain
(Received 24 March 2014; published 17 November 2014)

The violation of the Cauchy-Schwarz and Bell inequalities ranks among the major evidence of the genuinely quantum nature of an emitter. The conventional theoretical approaches associate operators with spectral lines to study correlations between photons from real-state transitions. Instead, we use a formalism that studies directly correlations between the physical reality—the photons—with no prejudice as to their origin. This allows us to extend photon correlations to all frequencies in all the possible windows of detection and to reveal landscapes of two-photon correlations that delineate regions of quantum emission, i.e., where classical inequalities are violated. We show that quantum correlations are rooted in the joint emission of two photons involving virtual states of the emitter instead of, as previously assumed, cascaded transitions between real states. As a result, correlations can be optimized in a process akin to distillation by keeping only the emission which is quantum and filtering out that which is not.

DOI: 10.1103/PhysRevA.90.052111 PACS number(s): 03.65.Ud, 42.50.Ar, 42.50.Ct, 42.79.Ci

I. INTRODUCTION

Classical descriptions of the electromagnetic field [1] and local hidden variable theories [2] yield a series of inequalities that impose an upper limit on the correlations between two modes and whose violation proves unequivocally the nonclassical character of quantum mechanics [3]. Among such equalities, the Cauchy-Schwarz inequality (CSI) and Bell's inequalities (BIs) are prominent examples that have been scrutinized in a large and varied set of platforms. The CSI [4] is one of the most important relations in all of mathematics. It states that fluctuations of products of random variables are bounded by the product of autocorrelations: $|\langle XY\rangle| \leqslant \sqrt{\langle X^2\rangle\langle Y^2\rangle}$. When X and Y are quantum observables, however, this relation can be violated. That is, quantum correlations between two separate objects can be so strong as to overcome their individual fluctuations in a way that is unaccountable by classical physics. BIs, on the other hand, refer to the wider problem of the nonlocal character of quantum mechanics [5]. Their violation decides in favor of quantum theory over local hidden variable theories. The underlying correlations are well known to power quantum information processing [6].

The first experimental demonstrations of violation of these inequalities were realized in the 1970s, in the radiation of an atomic two-photon cascade, for the CSI [7] and in the early 1980s for the BIs [8,9]. There has been a large body of literature confirming and documenting such violations ever since [10–16]. Most experimental realizations in both cases involve the correlation of photons of different frequencies emitted in a multiphoton process, such as atomic cascades [8] and four-wave mixing [13,17]. In the underlying theoretical models, these photons are attributed to "decay operators" that correspond to specific optical transitions [3]. This facilitates the calculation of frequency correlations in terms of these operators. They are, however, abstract mathematical representations of the photons, the latter being the only physical reality perceived by the measuring devices. One can inquire what are the correlations between photons with a given property—typically, frequency for the CSI and polarization for the BIs—with no theoretical prejudice as to their origin in terms of underlying operators. For instance, one can ask what are the correlations from spectral windows that do not correspond to transitions that such a model can represent through suitable decay operators. In this text, we address this question in a general context for frequency correlations, but to fix ideas, we illustrate our claims with one particular source of photons. To emphasize that frequency-correlated photons do not need to be attached to different modes, we consider a single-mode emitter. The simplest nontrivial candidate—resonance fluorescence—is also of great intrinsic interest and has been a favorite test bed of quantum optics [18]. To make clear that this is a general theme that is not specific to this system, however, we also briefly discuss similar results in the Jaynes-Cummings dynamics [19].

II. FREQUENCY CORRELATIONS IN RESONANCE FLUORESCENCE

Resonance fluorescence refers to the light emitted under coherent driving by a two-level system (2LS) [20–22]. At a high pumping intensity, the luminescence spectrum splits into three peaks, known as the Mollow triplet [23] [cf. Fig. 1(a)]. While the emission comes from a single mode, σ, the distinctive spectral shape calls naturally to question what are the correlations of—and between—the three peaks. It has been suggested theoretically [24–27] and established experimentally [26,28,29] that the photons from the peaks are strongly correlated. The Hamiltonian for this system reads

$$H_0 = \omega_\sigma \sigma^\dagger\sigma + \Omega(e^{-i\omega_L t}\sigma^\dagger + e^{i\omega_L t}\sigma), \tag{1}$$

with ω_σ the energy of the 2LS and Ω the intensity of the field driving it with frequency ω_L. With little loss of generality we consider resonant excitation: $\omega_L = \omega_\sigma$. Dissipation for the emitter is included in the density matrix formalism as a Lindblad term $\mathcal{L}_\sigma\rho$ with decay rate γ_σ in the master

*carlossmwolff@gmail.com
†fabrice.laussy@gmail.com

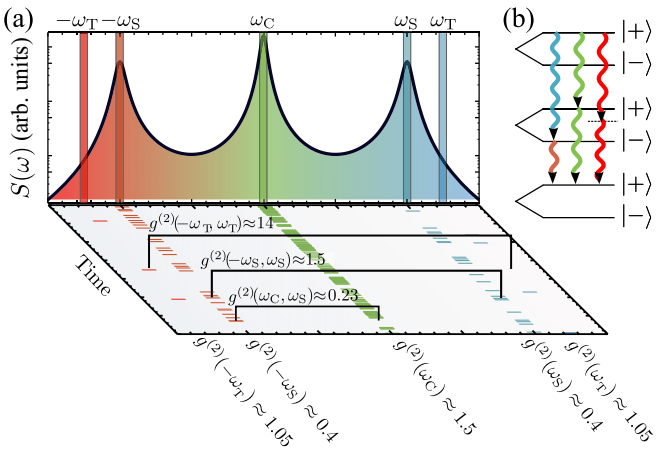

FIG. 1. (Color online) Violation of the CSI and BIs by frequency-resolved correlations. (a) Spectrum of resonance fluorescence, where filtering is illustrated in the tails (T), sidebands (S), and central peak (C) of the Mollow triplet. (b) Two-photon de-excitation between rungs of the Mollow ladder involve an intermediate real state (blue, orange, and green arrows) or a virtual state (red arrows). The latter type conveys CSI and BI violation. It is found in the flanks or between the peaks, where the signal is, however, weaker. Parameters: $\Omega = 10\gamma_\sigma$, $\Gamma = \gamma_\sigma$, $\omega_S \approx 2\ \Omega$, $\omega_T = 2.5\ \Omega$.

equation [30]:

$$\dot{\rho} = -i[H_0,\rho] + \frac{\gamma_\sigma}{2}\mathcal{L}_\sigma\rho, \tag{2}$$

where $\mathcal{L}_\sigma\rho = 2\sigma\rho\sigma^\dagger - \sigma^\dagger\sigma\rho - \rho\sigma^\dagger\sigma$. One can solve this equation to obtain an analytical expression of the spectrum featuring the Mollow triplet [23,31], which, at resonance, presents a central peak and two sidebands at $\omega = \omega_L \pm \omega_S$, where

$$\omega_S = \mathrm{Re}\{\sqrt{(2\Omega)^2 - (\gamma_\sigma/4)^2}\}. \tag{3}$$

At this point, an *ad hoc* multiple-mode description is usually enforced out of the genuine single mode σ which, dressed by the laser, yields three types of transitions between the dressed states $|\pm\rangle$ [cf. Fig. 1(b)]. This allows us to introduce three auxiliary decay operators associated with the three peaks: $\sigma_1 = c^2|-\rangle\langle+|$, $\sigma_2 = cs[|+\rangle\langle+| - |-\rangle\langle-|]$, and $\sigma_3 = -s^2|+\rangle\langle-|$, with s and c two amplitudes [25,27]. One can easily compute correlations $\langle\sigma_i^\dagger\sigma_j^\dagger\sigma_j\sigma_i\rangle$ for $1 \leqslant i,j \leqslant 3$ among these operators, which are associated in the input-output formalism with those $\langle a_i^\dagger a_j^\dagger a_j a_i\rangle$ of the detected photons at a given frequency [32]. There are various shortcomings to this approach, which is an approximation rooted in the physical picture of the dressed atom. First, the identification of each photon to a given transition based on its frequency is a simplification. Although infrequent, it happens that a photon detected at the frequency of a given peak actually originates from the transition that chiefly accounts for another peak. When considering regions of overlap, such a misattribution can become a source of large errors. Second, this approach neglects interferences between photons that truly are emitted by the same mode σ. Third, operators defined in this way are usually noncommuting, and therefore correlations at zero delay can yield different results depending on the order of the operators [26]. Last, but not least, this approach also restricts the calculation to the three operators thus defined, while one can correlate any two frequency windows, of various widths and centered at arbitrary frequencies, not necessarily at the peak maxima.

III. THEORY OF FREQUENCY CORRELATIONS

To dispense with these approximations and constrains, an exact theory of frequency-resolved photon detection is required to correlate any two photons based only on their measured properties, with no assumption as to their origin or time of emission. The formal expression for the second-order correlation function between photons of two frequencies without resorting to contrived operators was formalized in the late 1980s [33,34]. We denote it $g_\Gamma^{(2)}(\omega_1,\omega_2)$. It provides the statistics of photons with frequencies ω_1 and ω_2 spectrally filtered in a Lorentzian window of width Γ. The resulting integral form turns out to be so awkward, however, that even in the possession of the expression, there was the need to return to the auxiliary operator approximation to compute it. In this paper, we use del Valle *et al.*'s theory of frequency-resolved photon correlations [35] to compute this measurable property exactly, with no intermediate artificial decay operators and, therefore, taking into account all the possible interferences and indistinguishability imposed by quantum mechanics. This theory establishes that frequency-resolved correlations of the light emitted by any open quantum system are the same as the correlations between "sensors" at these frequencies. These sensors are bosonic, commuting modes with annihilation operator a_i, $i = 1,2$, free energy ω_i, and decay rate Γ—accounting for the frequency linewidth of the sensors—which are weakly coupled to the emitting mode with a small coupling constant ε. They are included in the dynamics by the Hamiltonian term $H_S = \sum_i \omega_i a_i^\dagger a_i + \varepsilon(a_i^\dagger\sigma + a_i\sigma^\dagger)$ and Lindblad terms $\frac{\Gamma}{2}\sum_i \mathcal{L}_{a_i}\rho$ [35]. Frequency-resolved correlations are then computed as

$$g_\Gamma^{(2)}(\omega_1,\omega_2) = \lim_{\varepsilon\to 0}\frac{\langle a_1^\dagger a_2^\dagger a_2 a_1\rangle}{\langle a_1^\dagger a_1\rangle\langle a_2^\dagger a_2\rangle}. \tag{4}$$

With such a theoretical apparatus, a full mapping of the photon correlations can be obtained. For the case of the Mollow triplet, which we have chosen for illustration, the problem takes the vivid form pictured in Fig. 1. The spectral shape—the triplet—is represented on a log scale with a choice of five frequency windows, centered at $\pm\omega_T$ (tails), $\pm\omega_S$ (sidebands), and ω_C (central peak). A quantum Monte Carlo trajectory was calculated to simulate the photon detection events [36] for photodetectors measuring in these windows. The emitted photons in a small fraction of the trajectory are represented by ticks on the projected plane in Fig. 1(a). The intensities vary in each frequency window: there is of course more signal in the central peak than in the sidebands and more there than in the tails. What is of interest in quantum optics is the statistical distribution of, and the correlation between, these photons. The autocorrelation in a given window, shown in the lower part of Fig. 1(a), gives the statistics of emission of the stream of photons now defined by their mean frequency and spread. While the light emitted by the 2LS overall is perfectly

antibunched, one sees that with spectral filtering, one can "distill" light with different statistical properties [37], namely, (i) uncorrelated in the tails, (ii) antibunched in the satellite peaks, and (iii) bunched in the central peak. One can similarly calculate the cross-correlations between photons from two different windows, showing, this time, that photons from the satellites are positively correlated, $g^{(2)}_{\Gamma}(-\omega_S,\omega_S) \approx 1.5$, while photons from one satellite and the central peak are anticorrelated, with $g^{(2)}_{\Gamma}(\omega_C,\omega_S) \approx 0.23$. It is noteworthy here that the stronger correlations come from the tail events, with $g^{(2)}_{\Gamma}(-\omega_T,\omega_T) \approx 14$ for the window chosen and increasing with greater still separations. The price to pay for these strong correlations is a correspondingly vanishing signal. Events are rarer, but the strength of their correlations is increased. This is a general trend.

IV. VIOLATION OF CAUCHY-SCHWARZ AND BELL'S INEQUALITIES BY FREQUENCY FILTERING

In a quantum optical context, the CSI and BIs can be expressed through the correlators $\langle a_i^\dagger a_j^\dagger a_j a_i\rangle$, with $i,j \in \{1,2\}$, of two electromagnetic modes, a_1 and a_2. In terms of Glauber's second-order correlation functions at zero delay, $g^{(2)}_{ij} = \langle a_i^\dagger a_j^\dagger a_j a_i\rangle / (\langle a_j^\dagger a_j\rangle \langle a_i^\dagger a_i\rangle)$ [38], the CSI reads $[g^{(2)}_{12}]^2 \leqslant g^{(2)}_{11} g^{(2)}_{22}$. This can be expressed in terms of a ratio R that quantifies the degree of CSI violation,

$$R = \left[g^{(2)}_{12}\right]^2 / \left[g^{(2)}_{11}\, g^{(2)}_{22}\right], \tag{5}$$

so the CSI takes the form

$$R \leqslant 1. \tag{6}$$

One can use definition (4) for the cross correlations of Eq. (5) to obtain a degree of CSI violation $R_\Gamma(\omega_1,\omega_2)$ for frequency-filtered light.

The case of the BIs is less straightforward but can be cast in the same form. In the CHSH framework [39], one considers correlated pairs of particles. One of these particles enters an apparatus where an observable A_θ is measured, while the other particle enters another apparatus where an observable B_ϕ is measured. θ and ϕ are adjustable parameters of the apparatuses, e.g., a polarization angle. The results of each measurement must be dichotomic, i.e., in each apparatus, the particle must select one of two possible channels of the observables, providing values ± 1 (in some units) with probabilities $P^{(A_\theta)}_{\pm}$ and $P^{(B_\phi)}_{\pm}$, respectively. Therefore, the measurement in each apparatus yields the mean values $\langle A_\theta\rangle = P^{(A_\theta)}_{+} - P^{(A_\theta)}_{-}$ and $\langle B_\phi\rangle = P^{(B_\phi)}_{+} - P^{(B_\phi)}_{-}$. As a consequence of this dichotomic character, the correlation $E(\theta,\phi) = \langle A_\theta B_\phi\rangle$ between both observables reads

$$E(\theta,\phi) = P^{(A_\theta,B_\phi)}_{++} + P^{(A_\theta,B_\phi)}_{--} - P^{(A_\theta,B_\phi)}_{+-} - P^{(A_\theta,B_\phi)}_{-+}, \tag{7}$$

where $P^{(A_\theta,B_\phi)}_{\pm\pm}$ is the joint probability of measuring $A_\phi = \pm 1$ and $B_\phi = \pm 1$. From this expression in a local hidden variable theory, one can derive a BI in the CHSH form [3,39],

$$B \leqslant 2, \tag{8}$$

where

$$B = |E(\theta,\phi) - E(\theta,\phi') + E(\theta',\phi') + E(\theta',\phi)|. \tag{9}$$

To clarify these concepts, we first consider the case usually discussed, in which the particles being correlated are photons and the measurements are done in the polarization degree of freedom. By the nature of the observable, $P^{(A_\theta)}_{\pm}$ corresponds to the fraction of the total intensity at both output arms of a polarizing beam splitter,

$$P^{A_\theta}_{\pm} = \langle I^{(A_\theta)}_{\pm}\rangle / \langle I^{(A_\theta)}_{+} + I^{(A_\theta)}_{-}\rangle\,, \tag{10}$$

where the adjustable parameter θ corresponds to the polarization angle. Correspondingly, the joint probability reads

$$P^{A_\theta,B_\phi}_{\pm\mp} = \frac{\langle I^{(A_\theta)}_{\pm} I^{(B_\phi)}_{\mp}\rangle}{\langle (I^{(A_\theta)}_{+} + I^{(A_\theta)}_{-})(I^{(B_\phi)}_{+} + I^{(B_\phi)}_{-})\rangle}\,, \tag{11}$$

and therefore, we can write $E(\theta,\phi)$ as

$$E(\theta,\phi) = \frac{\langle (I^{(A_\theta)}_{+} - I^{(A_\theta)}_{-})(I^{(B_\phi)}_{+} - I^{(B_\phi)}_{-})\rangle}{\langle (I^{(A_\theta)}_{+} + I^{(A_\theta)}_{-})(I^{(B_\phi)}_{+} + I^{(B_\phi)}_{-})\rangle}\,. \tag{12}$$

This is the typical situation when measuring BI violations for states of the type

$$|\psi\rangle = \frac{1}{\sqrt{2}}(a^\dagger_{1+}a^\dagger_{2+} + a^\dagger_{1-}a^\dagger_{2-})|0\rangle, \tag{13}$$

where $a^\dagger_{i,\pm}$ is the creation operator for a photon with polarization $\pm$ along path i, i.e., for states that are entangled.

In our work, we focus on the correlations from the output of a dynamical process, that is, we do not restrict ourselves to deterministic pure states [3] but consider a steady state as an input. This means that the intensities $I^{(A_\theta/B_\phi)}_{\pm}$ are not restricted to unity but can take any positive value. Moreover, we focus on a different scenario that does not involve the polarization degree of freedom, but only two modes states of the type $|\psi\rangle = a^\dagger_1 a^\dagger_2|0\rangle$. When disposing of an emitter that provides such a two-mode output, it can immediately be brought into an entangled form,

$$|\psi\rangle = \tfrac{1}{2}(a^\dagger_{1+}a^\dagger_{2+} - a^\dagger_{1-}a^\dagger_{2-} + i a^\dagger_{1-}a^\dagger_{2+} + i a^\dagger_{1+}a^\dagger_{2-})|0\rangle, \tag{14}$$

by placing two beam splitters across paths 1 and 2. The subscripts $\pm$ then refer to path instead of polarization. By recombining the four resulting beams in two additional beam splitters with variable transmittivities, which act as the apparatuses measuring A_θ and B_ϕ, these states can also violate the BIs by following the same line of reasoning as exposed above [3,39]. θ and ϕ represent, in this case, the tunable transmittivities of the two final beam splitters.

The setup implementing such a scheme of BI based on frequency filtering is sketched in Fig. 2, where the path degree of freedom 1,2 is associated with the energy degree of freedom ω_1,ω_2 using frequency filters. The two possible channels of detection in each final beam splitter are then equivalent to the two output ports of the polarizing filters of the conventional case, and the arguments that led to Eqs. (10) and (11) apply similarly. In a quantum-mechanical treatment, the modes at

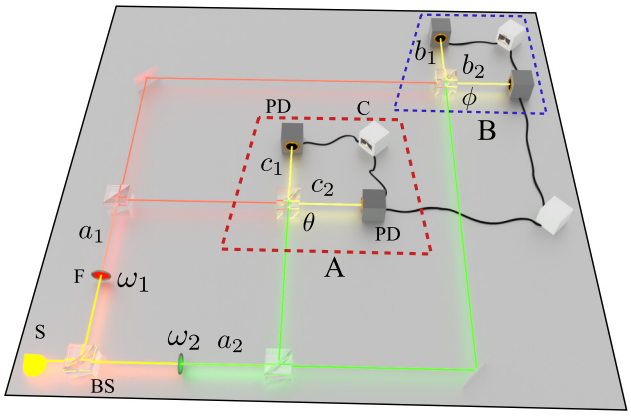

FIG. 2. (Color online) Test for the violation of Bell inequalities by frequency filtering. A source (S) emits photons in a broadband of frequencies. Frequency filters (F) select light at frequencies ω_1 and ω_2, described by the operators a_1 and a_2. Recombination at beam splitters (BS) with transmittivities given by $\sin\theta$ and $\sin\phi$ gives a total of four output beams, which are collected at the photodetectors (PD) and correlated with coincidence counters (C). Alice (A) and Bob (B) test nonlocality by independently measuring the probability of detection at the output ports of the two beam splitters, $P_{\pm}^{A_\theta}$ and $P_{\pm}^{B_\phi}$.

the output arms of the beam splitters are given by

$$\begin{aligned} c_1 &= \cos\theta a_1 + \sin\theta a_2, \quad c_2 = -\sin\theta a_1 + \cos\theta a_2, \\ b_1 &= \cos\phi a_1 - \sin\phi a_2, \quad b_2 = \sin\phi a_1 + \cos\phi a_2, \end{aligned} \tag{15}$$

and $E(\theta,\phi)$ takes the form

$$E(\theta,\phi) = \frac{\langle : (c_1^\dagger c_1 - c_2^\dagger c_2)(b_1^\dagger b_1 - b_2^\dagger b_2) : \rangle}{\langle : (c_1^\dagger c_1 + c_2^\dagger c_2)(b_1^\dagger b_1 + b_2^\dagger b_2) : \rangle}. \tag{16}$$

We adopt the standard choice of angles, which provides the greatest violation of the inequality: $\theta = 0, \phi = \pi/8, \theta' = \pi/4$, $\phi' = 3\pi/8$. This yields the following expression for B:

$$B = \sqrt{2}\left| \frac{\langle a_1^{\dagger 2} a_1^2 \rangle + \langle a_2^{\dagger 2} a_2^2 \rangle - 4\langle a_1^\dagger a_2^\dagger a_2 a_1 \rangle - \langle a_1^{\dagger 2} a_2^2 \rangle - \langle a_2^{\dagger 2} a_1^2 \rangle}{\langle a_1^{\dagger 2} a_1^2 \rangle + \langle a_2^{\dagger 2} a_2^2 \rangle + 2\langle a_1^\dagger a_2^\dagger a_2 a_1 \rangle} \right|. \tag{17}$$

It is equally easy to formulate these concepts in terms of frequency correlations as for the CSI. The operators a_1 and a_2 in Eq. (15) can be replaced with the sensor operators previously introduced and employed in Eq. (4), thus describing the light emitted at the two frequencies ω_1 and ω_2, as shown in Fig. 2. Direct application of Eq. (17) with these sensors a_i, whose finite linewidth Γ is described by their decay rate, provides $B_\Gamma(\omega_1,\omega_2)$.

V. RESULTS

A. Resonance fluorescence

At this point, we have set the stage to fully characterize the quantumness of the emission in terms of violation of the CSI and BIs spanning all the frequencies of emission and windows of detection. Note the considerable improvement compared to the approach that assigns a decay operator to each spectral line, since a continuum of frequencies in windows of arbitrary sizes can now be investigated without assumptions about the order of emission. Figure 3 shows three correlation landscapes in the frequency domain depicting the value of $g_\Gamma^{(2)}(\omega_1,\omega_2)$, $R_\Gamma(\omega_1,\omega_2)$, and $B_\Gamma(\omega_1,\omega_2)$ for three values of the detector linewidth in an otherwise identical configuration. An animation of the full landscapes of correlations as a function of the linewidth of filtering is provided in the Supplemental Material [40]. It is immediately apparent that the quantum character of the emission, where the inequalities are violated, is structured along three antidiagonals. In particular, the anticorrelation $g_\Gamma^{(2)}(\omega_1,\omega_2) < 1$ [corresponding to the blue areas in Fig. 3(a)] is a CSI violation in time when $\omega_1 = \omega_2$ and therefore corresponds to a nonclassical effect [41]. It makes no such guarantee, however, of a genuine quantum nature when $\omega_1 \neq \omega_2$ and, in fact, could even be produced by a classical emitter [42]. The corresponding CSI violation in time in this case is $[g_\Gamma^{(2)}(\tau,\omega_1,\omega_2)]^2 > g_\Gamma^{(2)}(0,\omega_1,\omega_1)g_\Gamma^{(2)}(0,\omega_2,\omega_2)$, which we study at zero time delay $\tau = 0$ in Fig. 3(b). Comparing these two rows, one can see that the regions of CSI violation correspond not to frequency antibunching but, quite the opposite, to frequency bunching. The reason for this lies in the nature of the violation, with cross-correlations being higher with respect to autocorrelations than permitted by classical physics. Physically, the antidiagonals where this happens are precisely those where two-photon emission occurs in a "leapfrog process" [43], i.e., a jump over the intermediate real state by involving a virtual state instead. This generates the state $|11\rangle$, which, fed to beam splitters, generates the maximally entangled state that optimizes the violation. The antidiagonal, line I, corresponds to transitions from $|+\rangle$ to $|+\rangle$ or from $|-\rangle$ to $|-\rangle$, two rungs below, as sketched in Fig. 1(b), thus satisfying $\omega_1 + \omega_2 = 0$. Line II and its symmetric correspond to transitions from $|+\rangle$ to $|-\rangle$ and from $|-\rangle$ to $|+\rangle$, respectively, satisfying $\omega_1 + \omega_2 = \pm\omega_S$. The CSI and BIs are less, or are not, violated whenever the intermediate rung intersects a real state, as shown by the fact that the green (for R_Γ) and red (for B_Γ) regions are depleted or pierced when intersecting the sidebands $\pm\omega_S$. This is particularly important since previous studies have focused precisely on correlations between real transitions, i.e., between peaks, such as indicated by the red square in the rightmost panel in Fig. 3(a). Instead, the exact treatment shows that these are detrimental to the effect, that is optimum when involving virtual states, since these are the vector of quantum correlations. It is easy to prove, from the closed form expression Eqs. (6)–(8) in Ref. [43], that a single-mode emitter with no dressing (here by the laser) never violates the CSI, regardless of the frequencies and detection widths. The same was checked numerically for the case of the BIs. Notably, this is true even if the emitter is a 2LS and exhibits perfect antibunching, $g^{(2)}(\tau = 0) = 0$. All this evidence confirms that CSI and BI violations are rooted in the quantum dynamics that involves a virtual state in a collective de-excitation in the quantum ladder of the dressed states. Here, one must keep in mind that there is only one emitter, so collectivity does not refer to the cooperation of multiple emitters, as is usually the case with effects such as superradiance [44], but refers to the joint action of multiple excitations of the one emitter. In our case, indeed, two photons team up to undergo a de-excitation that they can only realize

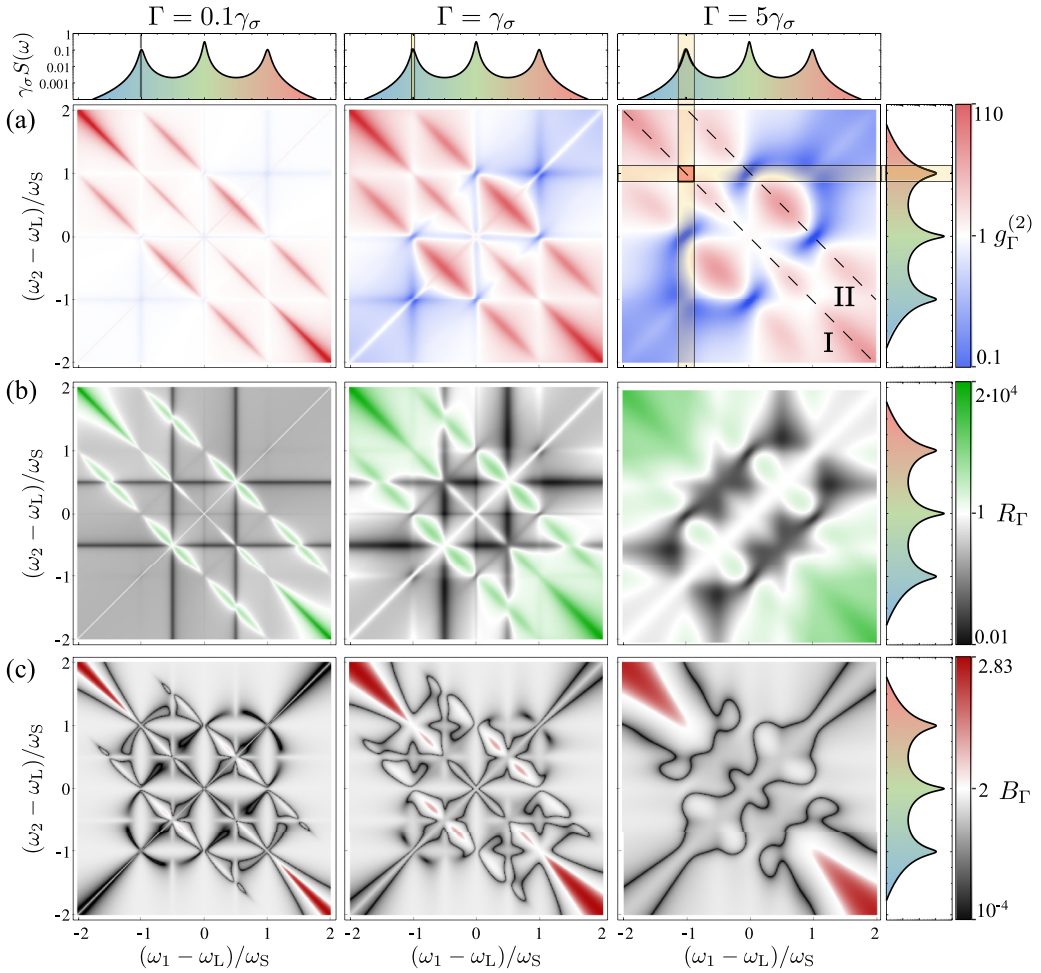

FIG. 3. (Color online) Landscapes of correlations in the frequency domain for three filter linewidths: (a) $g_\Gamma^{(2)}(\omega_1,\omega_2)$, (b) $R_\Gamma(\omega_1,\omega_2)$, and (c) $B_\Gamma(\omega_1,\omega_2)$. In (b) [(c)], the color code is such that green [red] violates the CSI [BI] and thus corresponds to genuine quantum correlations between the detected photons in the corresponding energy windows, while black and white do not (with white maximizing the inequality). The violation originates from the emission that involves virtual states. Dashed lines I and II in (a) are the cuts in the frequency domain along which the curves in Fig. 4 are calculated. Spectra on the axes show which frequency windows are correlated. Parameters are the same as in Fig. 1. An animation of these landscapes as a function of the detector linewidth is provided in the Supplemental Material [40].

together. Such pairs of photons are at the origin of the quantum emission: other types of de-excitation, which are not collective in this sense, do not violate the classical inequalities.

A more quantitative reading of these results is given in Figs. 4(a) and 4(b), which shows slices in the landscapes along lines I and II in the rightmost panel in Fig. 3(a). The quantum correlations violating the CSI are found in the side peaks and beyond, being larger the farther they are from the peaks. The same feature is present in the BI violation, which, furthermore, tends to the maximum value allowed, $B_\Gamma = 2\sqrt{2}$. Figures 4(c) and 4(d) show $g_\Gamma^{(2)}(\omega,\omega)$ and $g_\Gamma^{(2)}(\omega,-\omega)$—which can be used to derive $R_\Gamma(\omega,-\omega)$ and an approximation of $B_\Gamma(\omega,-\omega)$ [45]—as calculated exactly [solid (red) lines] [35,43] and through the approximation of auxiliary decay operators used in previous works [dashed (blue) lines] [26,27]. In such an approximation, the estimation is local around the peaks, that is, at $\omega/\omega_S = \pm 1$ and 0, where it is seen to be fairly accurate indeed, although not numerically exact. It can still lead to qualitative error, e.g., the autocorrelation at the sidebands is exactly 0 in this approximation, predicting arbitrary violation of the CSI even when it is obeyed. A violation of the BIs was also predicted [46], however, it was considered ill defined due to the perfect antibunching of the sidebands. Furthermore, these expressions are found in limiting cases for the filter linewidths: either $\Gamma \ll \gamma_\sigma \ll \Omega$ or $\gamma_\sigma \ll \Gamma \ll \Omega$. Both assume that the peaks are well separated to allow for the auxiliary operator approximation. They predict no CSI or BI violation for narrow filters, which is ultimately verified, although in the case of CSI, it is for values of the detector linewidth so small that they are unphysical. Solid lines in Fig. 5(a) show the dependence of R_Γ and B_Γ on the detector linewidth Γ for the three sets of frequencies $(\omega_i, -\omega_i)$, $i \in 1,2,3$, depicted in Fig. 5(b). For the already extremely small value of frequency windows $\Gamma = 0.1\gamma_\sigma$, the CSI and BIs can be violated, in contradiction with the prediction of the auxiliary operator approximation.

There are mainly three regimes of frequency correlations: narrow filters, peak filtering, and overlapping windows. While narrow filters better define the structure, as shown in Fig. 3, they also correspond to longer times of integration due to

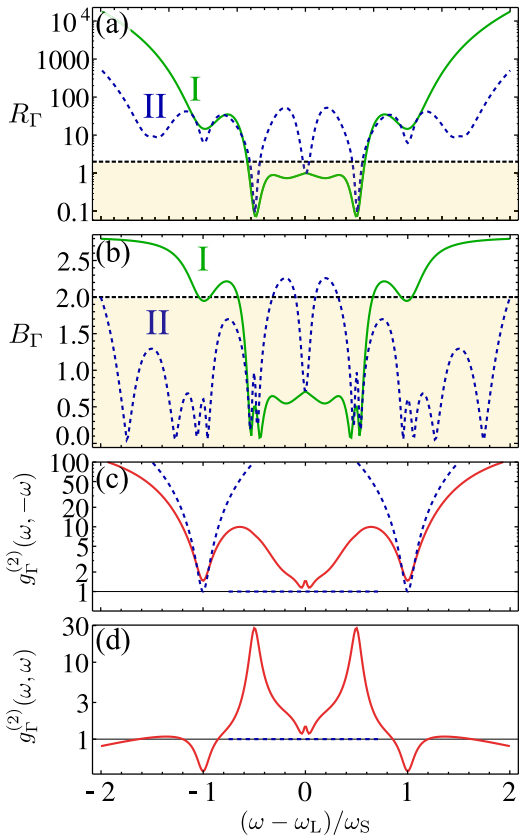

FIG. 4. (Color online) (a, b) Cuts of R_Γ (a) and B_Γ (b) along lines I $(\omega, -\omega)$ and II $(\omega,\omega_S-\omega)$ in Fig. 3(a). Parameters are the same as in Fig. 1, with $\Gamma=\gamma_\sigma$. (c, d) Photon correlation $g^{(2)}_\Gamma(\omega,\pm\omega)$ computed exactly [solid (red) lines] or through the usual auxiliary operator approximation [dashed (blue) lines]. In (d), the absence of the latter curve in some domains corresponds to values which are, incorrectly, exactly 0 (the vertical axis is on log scale).

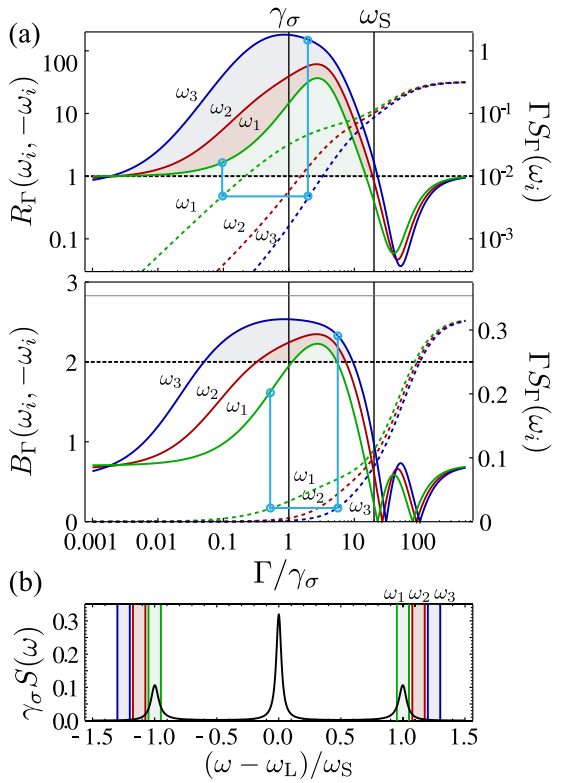

FIG. 5. (Color online) (a) Solid lines: $R_\Gamma(\omega_i,-\omega_i)$ (top) and $B_\Gamma(\omega_i,-\omega_i)$ (bottom) as a function of the detector linewidth for the three sets of frequencies $(\omega_i,-\omega_i)$, $i\in 1,2,3$, depicted in (b). Dashed lines: Amount of signal $\Gamma S_\Gamma(\omega)$ that can be collected for the corresponding filter linewidth. Filled (blue) circles illustrate how two configurations with the same amount of collected signal can yield different degrees of violation. (b) Resonance fluorescence spectrum, this time on a linear scale, displaying the characteristic Mollow triplet and three sensors with linewidth $\Gamma=2\gamma_\sigma$ centered at the frequencies used for (a): $\omega_1=\omega_S$, $\omega_2=1.125\,\omega_S$, and $\omega_3=1.25\,\omega_S$. Parameters are the same as in Fig. 1.

the time-frequency uncertainty and thus average out the correlations. A maximum is found when filtering in windows of the order of the peak linewidth or above, which is a welcomed result for an experimentalist. The overlap of the filters marks a change of trend in all the curves, due to a competition between various phenomena involving, for instance, various transitions as well as averaging over different types of interferences. Dashed lines in Fig. 5(a) show the value of $\Gamma S_\Gamma(\omega)$ corresponding to the amount of signal that can be collected with a detector of linewidth Γ at frequency ω [35]. In this way, one can easily compare, for a given amount of available signal, the different degrees of violation which are accessible simply by selecting the frequency and the window of the detector appropriately. Since such correlations are useful for technological purposes, the ability to compute the entire landscape of frequency correlations becomes helpful for optimizing quantum information processing. Correlations along line I of the map arise from a well-defined family of virtual processes, from which sideband correlations have been shown to be just a particular—and, in fact, also a detrimental—case. By positioning the filters away from the sidebands and increasing the frequency window of detection, it is possible to extract light showing stronger quantum correlations without any detrimental effect on the signal. In this way, one can optimize quantum correlations in a distillation process in which only photons with sought correlations are retained, and the others are filtered out.

B. Jaynes-Cummings

The previous results are general, as they relate to the added information one can gain from frequency filtering, rather than on the specificities of the source. While resonance fluorescence is a particular fruitful emitter with which to investigate such effects, the same principles apply in any other system that emits correlated photons and that has a spectral structure. To illustrate this point, we show in Fig. 6 similar features observed in the case of the Jaynes-Cummings model [19], in which a 2LS interacts with a single electromagnetic mode via the Hamiltonian $H=g(a^\dagger\sigma+a\sigma^\dagger)$ and with Lindblad terms to describe the incoherent pumping of the 2LS as well as decay of both the 2LS and the electromagnetic mode, leading to the Liouville equation $\dot\rho=-i[H,\rho]+(\frac{\gamma_\sigma}{2}\mathcal{L}_\sigma+\frac{\gamma_a}{2}\mathcal{L}_a+\frac{P_\sigma}{2}\mathcal{L}_{\sigma^\dagger})\rho$. The spectral shape of this system is the Rabi doublet at low pumping and a Jaynes-Cummings multiplet

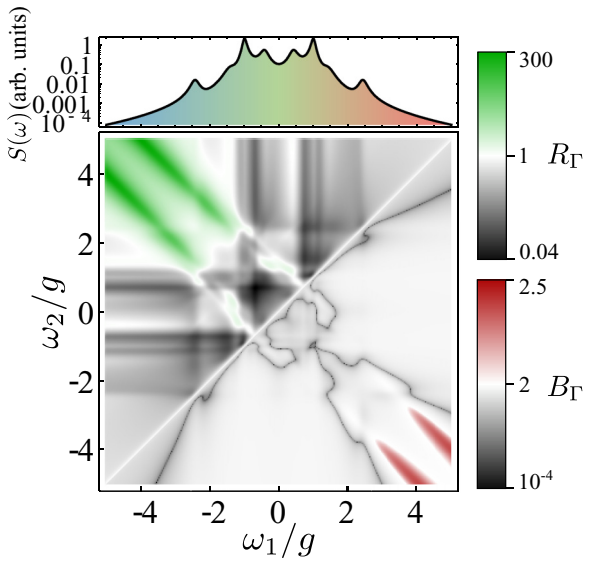

FIG. 6. (Color online) Landscapes of correlations for the Jaynes-Cummings model featuring violation of both the Cauchy-Schwarz inequality (upper left) and the Bell's inequalities (bottom right). The full landscape for each case follows by symmetry. Parameters: $\gamma_\sigma = 10^{-3}g$, $\gamma_a = 0.1g$, $P_\sigma = 0.05g$, and $\Gamma = 0.1g$.

when transitions from higher rungs get activated at higher pumping. In Fig. 6, one can observe how, again, regions of quantum emission appear along the lines that correspond to families of virtual two-photon processes in the Jaynes-Cummings ladder [43]. There is a region of CSI violation between the Rabi peaks but it is hindered by the proximity of real-state transitions. The BIs are, overall, more difficult to violate than in resonance fluorescence. At lower pumping, only the CSI violation survives, and with regions of quantum emission closely associated with those of photon bunching (not shown). A full analysis would bring us to the peculiarities of the Jaynes-Cummings dynamics and therefore goes beyond the scope of this text, which focuses on the principle of frequency filtering to optimize the violation of classical inequalities.

VI. CONCLUSIONS AND PERSPECTIVES

We have shown how to demonstrate and optimize CSI and BI violations between photons resolved in frequency from a quantum source, with no constraints or approximations from the theoretical description. Maximum violation is to be found not when correlating peaks in the spectrum, as previously thought, and thus linked to transitions between real states, but when involving virtual processes in the quantum dynamics. These results show the potential of frequency correlations to engineer quantum correlations and could be applied towards the design of optimum quantum information processing devices.

ACKNOWLEDGMENTS

We acknowledge the IEF project SQUIRREL (623708), the Spanish MINECO (MAT2011-22997, FPI and RyC programs), and the POLAFLOW European Research Council starting grant.

[1] R. Loudon, Rep. Prog. Phys. **43**, 913 (1980).
[2] J. S. Bell, Rev. Mod. Phys. **38**, 447 (1966).
[3] M. D. Reid and D. F. Walls, Phys. Rev. A **34**, 1260 (1986).
[4] G. Hardy, J. Littlewood, and G. Pólya, *Inequalities*, 2nd ed. (Cambridge Mathematical Library, Cambridge, 1952).
[5] A. Aspect, Sémin. Poincaré **XVII**, 99 (2013).
[6] A. K. Ekert, Phys. Rev. Lett. **67**, 661 (1991).
[7] J. F. Clauser, Phys. Rev. D **9**, 853 (1974).
[8] A. Aspect, P. Grangier, and G. Roger, Phys. Rev. Lett. **47**, 460 (1981).
[9] A. Aspect, J. Dalibard, and G. Roger, Phys. Rev. Lett. **49**, 1804 (1982).
[10] M. A. Rowe, D. Kielpinski, V. Meyer, C. A. Sackett, W. M. Itano, C. Monroe, and D. J. Wineland, Nature **409**, 791 (2001).
[11] A. Kuzmich, W. P. Bowen, A. D. Boozer, A. Boca, C. W. Chou, L.-M. Duan, and H. J. Kimble, Nature **423**, 731 (2003).
[12] V. Balić, D. A. Braje, P. Kolchin, G. Y. Yin, and S. E. Harris, Phys. Rev. Lett. **94**, 183601 (2005).
[13] J. K. Thompson, J. Simon, H. Loh, and V. Vuletić, Science **313**, 74 (2006).
[14] H. Sakai, T. Saito, T. Ikeda, K. Itoh, T. Kawabata, H. Kuboki, Y. Maeda, N. Matsui, C. Rangacharyulu, M. Sasano *et al.*, Phys. Rev. Lett. **97**, 150405 (2006).
[15] A. M. Marino, V. Boyer, and P. D. Lett, Phys. Rev. Lett. **100**, 233601 (2008).
[16] K. V. Kheruntsyan, J.-C. Jaskula, P. Deuar, M. Bonneau, G. B. Partridge, J. Ruaudel, R. Lopes, D. Boiron, and C. I. Westbrook, Phys. Rev. Lett. **108**, 260401 (2012).
[17] B. Srivathsan, G. K. Gulati, B. Chng, G. Maslennikov, D. Matsukevich, and C. Kurtsiefer, Phys. Rev. Lett. **111**, 123602 (2013).
[18] H. J. Kimble and L. Mandel, Phys. Rev. A **13**, 2123 (1976).
[19] E. Jaynes and F. Cummings, Proc. IEEE **51**, 89 (1963).
[20] E. B. Flagg, A. Muller, J. W. Robertson, S. Founta, D. G. Deppe, M. Xiao, W. Ma, G. J. Salamo, and C. K. Shih, Nat. Phys. **5**, 203 (2009).
[21] O. Astafiev, A. M. Zagoskin, A. A. Abdumalikov Jr., Y. A. Pashkin, T. Yamamoto, K. Inomata, Y. Nakamura, and J. S. Tsai, Science **327**, 840 (2010).
[22] P. Lodahl, S. Mahmoodian, and S. Stobbe, arXiv:1312.1079.
[23] B. R. Mollow, Phys. Rev. **188**, 1969 (1969).
[24] C. Cohen-Tannoudji and S. Reynaud, Phil. Trans. R. Soc. Lond. A **293**, 223 (1979).
[25] P. A. Apanasevich and S. Y. Kilin, J. Phys. B.: At. Mol. Phys. **12**, L83 (1979).
[26] C. A. Schrama, G. Nienhuis, H. A. Dijkerman, C. Steijsiger, and H. G. M. Heideman, Phys. Rev. A **45**, 8045 (1992).
[27] G. Nienhuis, Phys. Rev. A **47**, 510 (1993).

[28] A. Aspect, G. Roger, S. Reynaud, J. Dalibard, and C. Cohen-Tannoudji, Phys. Rev. Lett. **45**, 617 (1980).
[29] A. Ulhaq, S. Weiler, S. M. Ulrich, R. Roßbach, M. Jetter, and P. Michler, Nat. Photon. **6**, 238 (2012).
[30] H.-P. Breuer and F. Petruccione, *The Theory of Open Quantum Systems* (Oxford University Press, New York, 2002).
[31] E. del Valle and F. P. Laussy, Phys. Rev. Lett. **105**, 233601 (2010).
[32] G. W. Gardiner and P. Zoller, *Quantum Noise*, 2nd ed. (Springer-Verlag, Berlin, 2000).
[33] L. Knöll and G. Weber, J. Phys. B.: At. Mol. Phys. **19**, 2817 (1986).
[34] J. D. Cresser, J. Phys. B.: At. Mol. Phys. **20**, 4915 (1987).
[35] E. del Valle, A. Gonzalez-Tudela, F. P. Laussy, C. Tejedor, and M. J. Hartmann, Phys. Rev. Lett. **109**, 183601 (2012).
[36] M. B. Plenio and P. L. Knight, Rev. Mod. Phys. **70**, 101 (1998).
[37] E. del Valle, New J. Phys. **15**, 025019 (2013).
[38] R. J. Glauber, Phys. Rev. **130**, 2529 (1963).
[39] J. F. Clauser, M. A. Horne, A. Shimony, and R. A. Holt, Phys. Rev. Lett. **23**, 880 (1969).
[40] See Supplemental Material at http://link.aps.org/supplemental/10.1103/PhysRevA.90.052111 for landscapes of correlations in the frequency domain for varying filter linewidths.
[41] R. Loudon, *The Quantum Theory of Light* (Oxford Science, New York, 2000).
[42] A. Gonzalez-Tudela, B. Silva, C. Sanchez Muñoz, E. del Valle, and F. P. Laussy (unpublished).
[43] A. Gonzalez-Tudela, F. P. Laussy, C. Tejedor, M. J. Hartmann, and E. del Valle, New J. Phys. **15**, 033036 (2013).
[44] A. V. Andreev, V. I. Emel'yanov, and Y. A. Il'inski, Sov. Phys. Usp. **23**, 493 (1980).
[45] An approximation for $B_\Gamma(\omega, -\omega)$ can be obtained by dropping the last two terms of the numerator in Eq. (17) [47]. This approximation can be applied as long as there is no second-order transfer of photons between the modes, but these terms could be important in other cases. We have verified that they are indeed negligible in our configuration.
[46] A. Joshi and S. V. Lawande, Phys. Rev. A **44**, 716 (1991).
[47] N. A. Ansari, Phys. Rev. A **55**, 1639 (1997).